Sliding window assessment for sensor fault model-based diagnosis in inland waterways

P. Segovia [*,**,***] **J. Blesa** [**] **E. Duviella** [***] **L. Rajaoarisoa** [***]
F. Nejjari [*] **V. Puig** [*,**]

[*] *Automatic Control Department, Technical University of Catalonia (UPC), Terrassa, Spain {pablo.segovia, fatiha.nejjari, vicenc.puig}@upc.edu*
[**] *Institut de Robòtica i Informàtica Industrial (CSIC-UPC), Barcelona, Spain {joaquim.blesa@upc.edu}*
[***] *URIA, IMT Lille Douai, France {pablo.segovia, eric.duviella, lala.rajaoarisoa}@imt-lille-douai.fr*

Abstract: The Cuinchy-Fontinettes reach belongs to the inland waterways in the north of France. It is equipped with limnimeters that measure water level data for the management of the water resources. These data can be corrupted by constant or intermittent faults. Hence, it is necessary to detect and localize these faults in order to guarantee efficient management actions. The proposed fault diagnosis method is based on the analysis of the parameters of a grey-box model. These parameters are obtained from available real data by using a sliding window, whose size is determined based on the level of excitation of input signals. Then, several scenarios involving constant and intermittent faults are proposed to discuss the performance of the proposed FDI approach as well as the effect of the sliding window size on the results.

Keywords: Large-scale systems, inland waterways, fault diagnosis, grey-box model.

1. INTRODUCTION

The Cuinchy-Fontinettes reach (CFr) belongs to the inland waterways in the north of France. It is equipped with controlled gates that are used to regulate the levels by dispatching volumes of water and with locks that make possible the navigation of boats along the waterway. The management condition to be fulfilled aims at keeping the water levels close to the setpoint, which is known as the normal navigation level (NNL). The design and implementation of control algorithms such as those proposed in (Segovia et al., 2017b; Horváth et al., 2014c) require the measurement of levels. However, these measurements can be corrupted by several types of faults, which can lead to undesired control actions. Thus, fault detection and isolation (FDI) techniques must be designed to detect and localize the faults. Blesa et al. (2010) proposed a fault detection method based on a linear parameter-varying (LPV) model in order to detect faults that occur in open-channel systems. Model-based method and intervals models have been proposed in (Segovia et al., 2017a; Blesa et al., 2014) respectively, for sensor fault detection in inland waterways. A comparison of FDI methods to detect leaks in an irrigation network has been carried out in (Bedjaoui and Weyer, 2011). Nabais et al. (2012) proposed another sensor FDI approach for irrigation canals based on residual generation. An unknown input observer (UIO) design for delayed LPV systems represented in the polytopic framework which has been applied to an open flow canal is proposed by Hassanabadi et al. (2016). FDI techniques based on classification techniques, black-box models or recursive subspace identification method have been proposed in (Pocher et al., 2011, 2012) and (Akhenak et al., 2013), respectively. A combination of a physical model and a classification algorithm has been designed in (Horváth et al., 2014a) and developed in (Duviella et al., 2013) by considering the grey-box model detailed in (Horváth et al., 2014b). In this paper, the FDI approach is based on the evolution of the grey-box parameters over the time. The parameters of the grey-box model are estimated based on real input/output data using a sliding window. Some rules to tune the length of the time window and guarantee the fitting of the identified model are proposed. The tuning of the time window length is discussed by considering real data from the CFr and three fault scenarios. The paper is organized as follows: the CFr and the management objectives are detailed in Section 2. The grey-box model is presented in Section 3. Section 4 describes the proposed FDI approach. Finally, the modeling and FDI techniques are illustrated in Section 5 by means of a case study.

⋆ The authors thank *Voies Navigables de France* for the data provided, which has made possible this work.

2. THE CUINCHY-FONTINETTES REACH

2.1 Management objectives

The CFr that is located in the north of France plays a crucial role in the transport and the water resources management of the waterways due to its location. During flood periods, the CFr is used to share water volumes between the Aa and the Lys watersheds. During drought periods, it is used to appropriately dispatch the available water resources among the watersheds. The objective is to make navigation possible during the arranged schedule. In order

to ensure the navigability of vessels, it is required that the water levels be inside the interval that is defined by considering a tolerance range around the NNL, *i.e.* lower and higher navigation levels (LNL and HNL, respectively).

2.2 Description

The CFr is 42 *km* long and delimited by the Cuinchy lock upstream and the Fontinettes lock downstream. It is equipped with gates in Cuinchy (beside the lock) and at Aire-sur-la-Lys with the gate of *Porte de Garde*, located 28 *km* downstream of Cuinchy (*see* Fig. 1), and with three limnimeters that allow measuring the water levels at Cuinchy (L^C), Aire-sur-la-Lys (L^A) and Fontinettes (L^F) with a sample time $k = 1$ *min*. The controlled discharges are applied by means of the Cuinchy lock and gate (Q^C), the *Porte de Garde* gate (Q^A) and the Fontinettes lock (Q^F). These magnitudes are measured each 15 *min*.

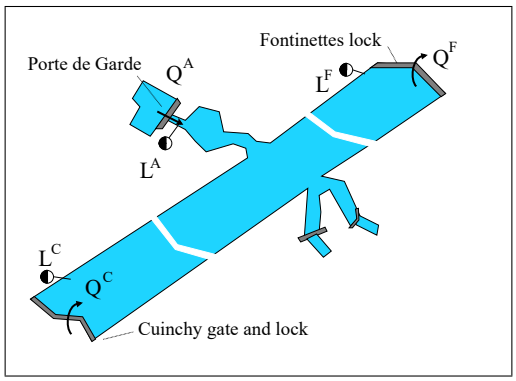

Fig. 1. Schematics of the CFr.

The CFr is an open-channel flow characterized by nonlinear dynamics with large time delays. In addition, its dynamics are impacted by strong resonance phenomena due to a negligible slope along its course. Lock operations create waves that travel back and forth along the reach during several hours until their attenuation.

2.3 Fault diagnosis in the CFr

In this system, faults mainly occur on sensors. They can be due to an offset error of the measurement during several hours (persistent faults), to transmission problems (intermittent faults) or to a combination of both (transient faults that lead to persistent faults). These faults can have a strong impact on the water level control, where the consideration of wrong data can lead to a system malfunction. Hence, sensor faults must be diagnosed. The main challenge of sensor fault diagnosis lies in the characteristics of the CFr: a large-scale system with nonlinear dynamics and large time delays. Moreover, when real data are considered, it is necessary to deal with strong uncertainties. While classical diagnosis approaches can face some difficulties, data-based approaches seem more suitable to deal with real data, as it was shown in (Duviella et al., 2013). The remaining task consists in detecting intermittent faults.

Thus, a grey-box model-based approach is designed to diagnose sensor faults by considering real data of the CFr, from October 30, 2013 (Thursday) to November 17, 2013 (Sunday). Part of these data are used to estimate the parameters of the grey-box model and determine the validity intervals of its main parameters. The remaining data are used to test the designed approach by introducing artificial faults.

3. GREY-BOX MODEL

3.1 Description

The structure of the grey-box model is a first order plus time delay for every input/output pair:

$$\hat{\boldsymbol{y}}_{k+1} = \boldsymbol{A}\overline{\boldsymbol{y}}_{k|\tau} + \boldsymbol{B}\overline{\boldsymbol{u}}_{k|\tau} \tag{1}$$

where input variables $\overline{\boldsymbol{u}}_{k|\tau} \in \mathbb{R}^{n^2\times 1}$ correspond to a combination of the components of the input vector $\boldsymbol{u}_k{=}[u_k^1 \dots u_k^n]^T$ with the corresponding delays, and $u_k^l = Q_k^l \ \forall l = 1, ..., n$ are the different discharges along the canal. Similarly, the output variables $\overline{\boldsymbol{y}}_{k|\tau} \in \mathbb{R}^{n^2\times 1}$ correspond to a combination of the components of the output vector $\boldsymbol{y}_k{=}[y_k^1 \dots y_k^n]^T$ with the corresponding delays, where $y_k^i = L_k^i \ \forall i = 1, ..., n$ are the different level measurements along the canal (*see* Fig. 2). Matrices $\boldsymbol{A} \in \mathbb{R}^{n\times n^2}$ and $\boldsymbol{B} \in \mathbb{R}^{n\times n^2}$ are defined under the assumption that each actuator is equipped with one limnimeter. The matrix $\boldsymbol{\tau} \in \mathbb{N}^{n\times n}$ given in Eq. (2) gathers the time delays between the measurement points L^i and L^j, and also between the discharge Q^i and the measurement point L^j, respectively. For instance, the value of $\tau_{i,j} \in \mathbb{N}$ is the time delay between the measurement points L^i (resp. Q^i) and L^j.

$$\boldsymbol{\tau} = \begin{bmatrix} 0 & \tau_{1,2} & \cdots & \tau_{1,n} \\ \tau_{2,1} & 0 & \cdots & \tau_{2,n} \\ \vdots & \vdots & \ddots & \vdots \\ \tau_{n,1} & \tau_{n,2} & \cdots & 0 \end{bmatrix} \tag{2}$$

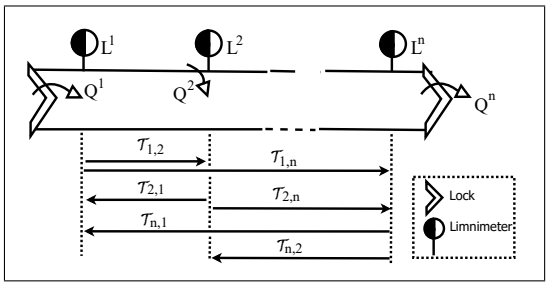

Fig. 2. Time delays $\tau_{i,j}$ between measurement points.

The time delays are determined according to the well-known relations given in (Litrico and Fromion, 2004).

The vector $\overline{\boldsymbol{y}}_{k|\tau}$ is expressed as:

$$\begin{aligned}\overline{\boldsymbol{y}}_{k|\tau} = [&L_k^1\ L_{k-\tau_{1,2}}^2 \cdots L_{k-\tau_{1,n}}^n\ L_{k-\tau_{2,1}}^1\ L_k^2 \cdots L_{k-\tau_{2,n}}^n \\ &\cdots L_{k-\tau_{n,1}}^1\ L_{k-\tau_{n,2}}^2 \cdots L_k^n]^T\end{aligned} \tag{3}$$

Likewise, $\overline{\boldsymbol{u}}_{k|\tau}$ reads as follows:

$$\begin{aligned}\overline{\boldsymbol{u}}_{k|\tau} = [&Q_k^1\ Q_{k-\tau_{1,2}}^2 \cdots Q_{k-\tau_{1,n}}^n\ Q_{k-\tau_{2,1}}^1\ Q_k^2 \cdots Q_{k-\tau_{2,n}}^n \\ &\cdots Q_{k-\tau_{n,1}}^1\ Q_{k-\tau_{n,2}}^2 \cdots Q_k^n]^T\end{aligned} \tag{4}$$

Matrix $\boldsymbol{A}$ is defined as the direct sum of vectors $\boldsymbol{A_{ii}}$, *i.e.* $\boldsymbol{A}{=}\bigoplus_{i=1}^{n}\boldsymbol{A_{ii}}$ ($\boldsymbol{B}$ is expressed similarly):

$$\boldsymbol{A} = \begin{bmatrix} \boldsymbol{A_{11}} & \boldsymbol{0_n} & \boldsymbol{0_n} & \boldsymbol{0_n} \\ \boldsymbol{0_n} & \boldsymbol{A_{22}} & \boldsymbol{0_n} & \boldsymbol{0_n} \\ & & \ddots & \\ \boldsymbol{0_n} & \boldsymbol{0_n} & & \boldsymbol{0_n} \\ \boldsymbol{0_n} & \boldsymbol{0_n} & \boldsymbol{0_n} & \boldsymbol{A_{nn}} \end{bmatrix} \tag{5}$$

with $\boldsymbol{A_{ii}} = \begin{bmatrix} a^{i,1} & \cdots & a^{i,n} \end{bmatrix}$ and $\mathbf{0_n}$ the zero vector of length n. $a^{i,i}$ is the parameter that links $\hat{y}^i_{k+1}$ to y^i_k with no delay.

Equation (1) is rewritten as follows:

$$\hat{\boldsymbol{y}}_{k+1} = \boldsymbol{M}\ \boldsymbol{\Phi}_k \tag{6}$$

with $\boldsymbol{M} = [\boldsymbol{A}\ \boldsymbol{B}]$ and $\boldsymbol{\Phi}_k = [\overline{\boldsymbol{y}}_{k|\tau}\ \overline{\boldsymbol{u}}_{k|\tau}]^T$. Then, $\boldsymbol{M}$ is the solution of the linear least squares problem. N samples of the measured discharges Q^i_k and levels L^i_k are considered in its computation:

$$\boldsymbol{M} = \boldsymbol{Y}\ \overline{\boldsymbol{\Phi}}^T\ (\overline{\boldsymbol{\Phi}}\ \overline{\boldsymbol{\Phi}}^T)^{-1} \tag{7}$$

with $\boldsymbol{Y} = [y_{\chi+1}\ \cdots\ y_N]$, $\overline{\boldsymbol{\Phi}} = [\boldsymbol{\Phi}_\chi\ \cdots\ \boldsymbol{\Phi}_{N-1}]$, and $\chi = \max(\boldsymbol{\tau}) + 1$, where $\max(\boldsymbol{\tau})$ is the maximum entry of matrix $\boldsymbol{\tau}$ given in (2).

3.2 Identification based on a sliding window

It is also possible to identify the parameters of the grey-box model by using sliding windows. In doing so, a model more reactive to changes and that follows more precisely the dynamics of the reach can be obtained. The value of $\boldsymbol{M}$ given in Eq. (7) is determined by considering a time window of size N_w. Hence, a temporal matrix $\boldsymbol{M}_k$ is computed at every instant k:

$$\boldsymbol{M}_k = \boldsymbol{Y}_k\ \overline{\boldsymbol{\Phi}}_k^T\ \left(\overline{\boldsymbol{\Phi}}_k\ \overline{\boldsymbol{\Phi}}_k^T\right)^{-1} \tag{8}$$

with $\boldsymbol{Y}_k = [y_{k+\chi+1-N_w} \cdots y_k]$, $\overline{\boldsymbol{\Phi}}_k = [\boldsymbol{\Phi}_{k+\chi-N_w} \cdots \boldsymbol{\Phi}_{k-1}]$.

The parameters $a^{j,i}_k$ and $b^{j,i}_k$ $\forall i, j = 1...n$ are obtained from $\boldsymbol{M}_k = [\boldsymbol{A}_k\ \boldsymbol{B}_k]$.

The time window N_w is tuned according to persistent excitation indicators in the inputs. The estimation of the parameters is done when the input persistent exciting order is high enough, as it is proposed in section 13.2 in (Ljung, 1999). The Matlab command *pexcit* is used to determine these indicators. There is no *a priori* maximum value of N_w. However, the larger N_w is, the lower the re-activity of the grey-box model would be, *i.e.* the modification time of the parameters' values would be bigger.

3.3 Validation step

The following fit coefficients are used to determine the accuracy of the grey-box model with respect to the measurements.

- *Pearson product-moment correlation coefficient* measures the linear dependence between two variables:

$$R^i = \frac{\sum_{k=1}^{N} \left(y^i_k - \lambda_{y^i}\right)\left(\hat{y}^i_k - \lambda_{\hat{y}^i}\right)}{\sqrt{\sum_{k=1}^{N} \left(y^i_k - \lambda_{y^i}\right)^2}\sqrt{\sum_{k=1}^{N} \left(\hat{y}^i_k - \lambda_{\hat{y}^i}\right)^2}} \tag{9}$$

  with λ_{y^i} and $\lambda_{\hat{y}^i}$ the mean value of measured and estimated water levels, respectively. This coefficient is bounded between +1 (total positive linear correlation) and -1 (total negative linear correlation), and 0 means that there is no linear correlation.
- *Nash-Sutcliffe model efficiency coefficient* is used to assess the predictive power of hydrological models (Nash and Sutcliffe, 1970):

$$E^i = 1 - \frac{\sum_{k=1}^{N} \left(y^i_k - \hat{y}^i_k\right)^2}{\sum_{k=1}^{N} \left(y^i_k - \lambda_{y^i}\right)^2} \tag{10}$$

  E^i can range from 1 to $-\infty$, where 1 indicates a perfect match of modeled and observed values, 0 corresponds to the case in which the model predictions are as accurate as the mean of observed data and $E^i < 0$ means that the model predictions are less accurate than the mean of observed data. It can also be expressed in percent when its value is positive.

Once the size of the time window N_w is tuned and the proposed model is validated, the coefficients of matrices $\boldsymbol{A}_k$ and $\boldsymbol{B}_k$ can be used to design the FDI strategy.

4. FAULT DIAGNOSIS

The fault diagnosis focuses on level sensor faults:

$$L^i_k = L^{i,0}_k + \Delta^i_k, \quad \forall i = 1, ..., n \tag{11}$$

where $L^{i,0}_k$ denotes the level i and Δ^i_k the fault at time k.

As (1) provides the level estimations $\hat{\boldsymbol{y}}_{k+1}$, the most straightforward fault detection method consists in evaluating the difference between the level sensor measurements and the estimations:

$$r^i_k = y^i_k - \hat{y}^i_k, \quad \forall i = 1, ..., n \tag{12}$$

where r^i_k is the temporal residual of the i-th level sensor. The fault detection test can be formulated as follows:

$$\phi^{r^i}_k = \begin{cases} 0 \text{ if } r^i_k \in [\underline{\sigma}^i, \overline{\sigma}^i] \Rightarrow \text{ No Fault} \\ 1 \text{ otherwise} \end{cases} \tag{13}$$

with bounds $\underline{\sigma}^i$ and $\overline{\sigma}^i$ the maximum positive and negative deviations of the residual r^i_k in a fault-free scenario.

A similar approach is followed by considering the grey-box model parameters. The main idea is that, under normal conditions, the dynamics of the reach are always similar, and therefore the parameters of the model fluctuate within a narrow interval. Hence, bounds are determined in a fault-free scenario for each parameter of matrix $\boldsymbol{M}_k$: $[\underline{a^{j,i}}, \overline{a^{j,i}}]$ and $[\underline{b^{j,i}}, \overline{b^{j,i}}]$. Conditions on persistent excitation and on the fitting indicators given in Eqs. (9)–(10) must be met. Thus, the parameter fault signals $\phi^{a^{j,i}}_k$ and $\phi^{b^{j,i}}_k$ can be generated in a similar way as $\phi^{r^i}_k$ in (13):

$$\phi^{a^{j,i}}_k = \begin{cases} 0 \text{ if } a^{j,i}_k \in [\underline{a^{j,i}}, \overline{a^{j,i}}] \Rightarrow \text{ no fault} \\ 1 \text{ otherwise} \end{cases} \tag{14}$$

$\phi^{b^{j,i}}_k$ is computed as $\phi^{a^{j,i}}_k$ but considering the parameter estimations $b^{j,i}_k$ and the bounds $[\underline{b^{j,i}}, \overline{b^{j,i}}]$ in (14).

A fault is detected when one fault signal $\phi^{a^{j,i}}_k$ or $\phi^{b^{j,i}}_k$ is activated, *i.e.* its value equals 1. The isolation of the fault benefits from the time delays that characterize the reach dynamics as proposed in (Puig and Blesa, 2013). Indeed, the effect of a fault in the limnimeter L^i (Δ^i_k) in the estimation of the level in the limnimeter L^j ($\hat{y}^j_k$) is delayed by $\tau_{i,j}$. For instance, when a fault Δ^i_k occurs, the temporal residual fault signal $\phi^{r^i}_k$ and the parametric fault signals $\phi^{a^{j,i}}_k$ and $\phi^{b^{j,i}}_k$ $\forall i = 1, \cdots, n$ should be activated in the first

place. In the case of parametric fault signals, the effect of the fault Δ_k^i is more direct on the estimation of parameter $a_k^{i,i}$. Next, the effect of the fault will be propagated to the nearest measurement point j, which will affect the estimation of the level and the parameters. As the effect of the fault Δ_k^i is attenuated in the propagation, it might be observed only in the nearest measurement points.

The estimation of the grey-box parameters is carried out by considering sliding windows of size N_w. Therefore, an extra delay between the fault occurrence and the effect in the fault signals is often present. By fulfilling the persistent excitation condition, the delay in the fault detection might be reduced using a smaller N_w. However, this improvement might be lost at the expense of the requirement of larger bounds on the parameters. It is thus necessary to reach a satisfactory trade-off between N_w and the detection time.

5. MODELLING AND FAULT DETECTION RESULTS

5.1 Modelling

Real data from the limnimeters and discharges are re-synchronized by considering a sampling time of 1 minute. Then, the delays between each part of the CFr are estimated according to the characteristics of the system (the values are in minutes):

$$\boldsymbol{\tau} = \begin{bmatrix} 0 & 78 & 115 \\ 79 & 0 & 37 \\ 116 & 37 & 0 \end{bmatrix} \tag{15}$$

According to these delays, the input and output vectors $\overline{\boldsymbol{u}}_{k|\tau} \in \mathbb{R}^9$ and $\overline{\boldsymbol{y}}_{k|\tau} \in \mathbb{R}^9$ are built by considering the following inputs and outputs: $u_k^1 = Q_k^C$, $y_k^1 = L_k^C$ for Cuinchy; $u_k^2 = Q_k^A$, $y_k^2 = L_k^A$ for Aire-sur-la-Lys; and $u_k^3 = Q_k^F$, $y_k^3 = L_k^F$ for Fontinettes.

To determine the minimum required size of the time window N_w, data from five consecutive days starting from October 30, 2013 (Thursday) are considered. Fig. 3 depicts the discharges and the levels in Cuinchy, Aire-sur-la-Lys and Fontinettes. The level of excitation of the input signals are computed for these data and depicted in Fig. 3.e for $N_w = 960$ (16 hours), $N_w = 1020$ (17 hours) and $N_w = 1440$ (24 hours). There is a peak of poor excitation level only for $N_w = 960$. For $N_w = 1020$ and $N_w = 1440$, the excitation levels are suitable and always equal to the maximum value 50. Figure 4 depicts the level of excitation of input signals *pexcit* according to N_w. It is shown that the minimal length of the window is $N_w = 963$. Thus, we consider that the minimal length of the window is $N_w = 1020$ corresponding to 17 hours. That means that at least 40 % of the data of N_w has to correspond to periods with lock operations.

The same data are used to identify a model for each window with $N_w = 1020$. The levels $\hat{L}_k^i$ are estimated as outputs of the grey-box model. The real measurements L_k^i and the estimated $\hat{L}_k^i$ are depicted in Fig. 5 in blue and dashed red lines, respectively, for each of the three limnimeters. Notice that these values are relative to the NNL, *i.e.* L_k^i=0 corresponds to the NNL in Fig. 5.

The Nash-Sutcliffe (E^i) and correlation (R^i) coefficients are computed and their average values for the three

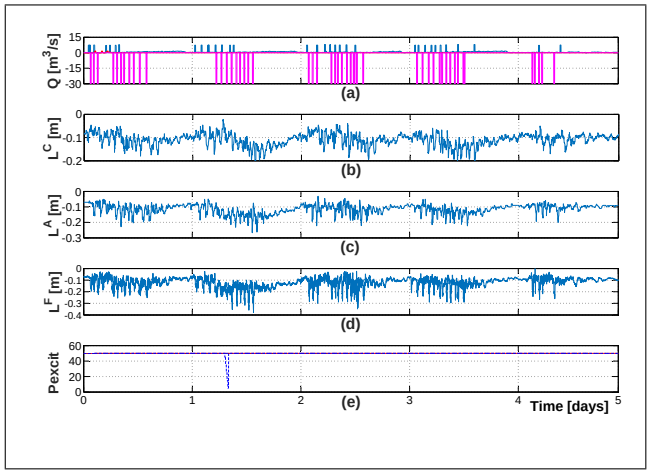

Fig. 3. (a) Discharges in Cuinchy (blue), Aire-sur-la-Lys (red) and Fontinettes (magenta). Water levels in: (b) Cuinchy. (c) Aire-sur-la-Lys. (d) Fontinettes. (e) Level of excitation of input signals, for $N_w = 960$ (blue), $N_w = 1020$ (red) and for $N_w = 1440$ (black).

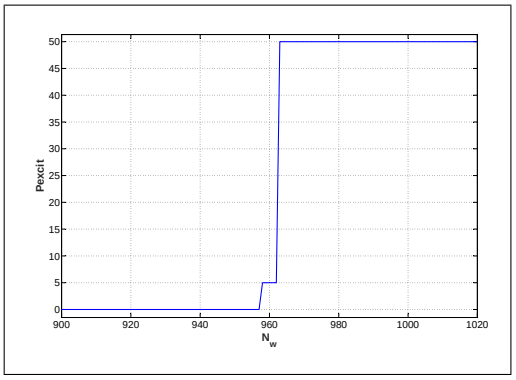

Fig. 4. Minimal level of excitation of input signals *pexcit* according to the window length N_w.

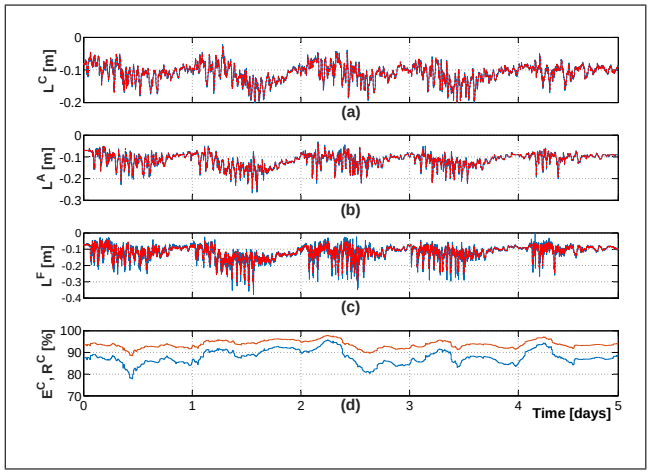

Fig. 5. Water levels in: (a) Cuinchy. (b) Aire-sur-la-Lys. (c) Fontinettes. Measured levels: blue solid line; estimated levels: red solid line with $N_w = 1020$. (d) Fit coefficients for Cuinchy.

limnimeters are given in Table 1 by considering the time window sizes $N_w = 1020$ and $N_w = 1440$. The quality of the models is confirmed in both cases even if it seems better for the largest time window. A time window of 24

hours ($N_w = 1440$) covers a whole day of navigation at each step time, which seems to be the main reason of the observed effectiveness of the models.

Table 1. Average values of Nash-Sutcliffe (E^i) and correlation (R^i) coefficients

	$N_w = 1020$		$N_w = 1440$	
Limnimeter	E^i [%]	R^i [%]	E^i [%]	R^i [%]
L^C	88	94	95	95
L^A	85	92	87	93
L^F	70	84	76	87

Finally, the identified parameters of the grey-box models for both time window sizes are depicted in Fig. 6 in red and blue lines, respectively. Their minimum and maximum values are computed to determine the intervals of the $a_k^{i,i}$ parameters. These values are depicted in dashed lines and are summarized in Table 2. As expected, the larger the time window is, the smaller the intervals are. These intervals will be used to detect and isolate faults.

Table 2. Boundaries on the grey-box models

	$N_w = 1020$		$N_w = 1440$	
Parameter	min	max	min	max
a^{11}	0.88	0.95	0.89	0.95
a^{22}	0.76	0.92	0.8	0.89
a^{33}	0.58	0.81	0.61	0.74

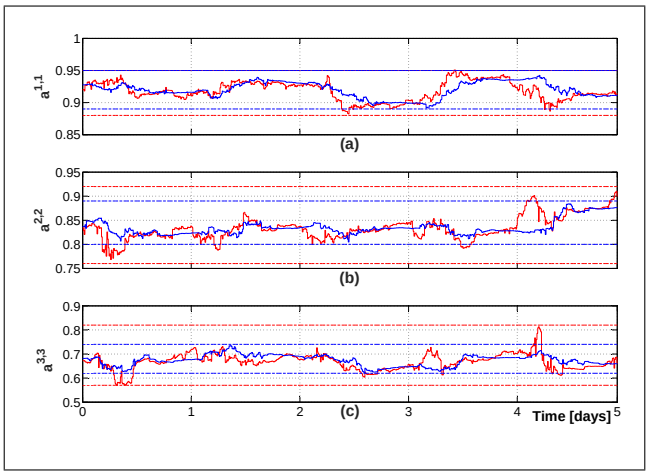

Fig. 6. Values of the $a_k^{i,i}$ parameters and determined thresholds: (a) $a^{1,1}$. (b) $a^{2,2}$. (c) $a^{3,3}$.

5.2 FDI in limnimeters

Levels from five consecutive days starting from November 12, 2013 (Tuesday) are considered in order to test the proposed FDI approach. Three faulty scenarios are created by adding artificial faults to the real measurements. Fault f_1 corresponds to a constant fault of -8 *cm* on the level L^C. Fault f_2 consists in an intermittent fault that becomes constant over time with a magnitude of 1.5 *cm* on the level L^A. This fault lasts until the end of the considered period of time. Fault f_3 is an intermittent fault with a magnitude of 5 *cm* on the level L^F during a bounded time. The features of the three faults are summarized in Table 3. The intermittent faults are generated according to Gaussian random signals, which means that two consecutive scenarios cannot be identical. Hence, 500 simulations based on

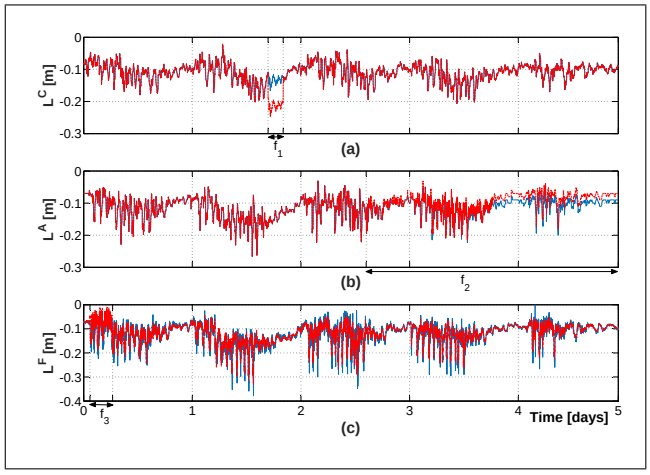

Fig. 7. Water levels in: (a) Cuinchy. (b) Aire-sur-la-Lys. (c) Fontinettes. Measured levels in blue solid line (free-fault case), in red dashed line (impacted by faults).

the Monte Carlo approach are performed to determine the average, minimum and maximum fault detection delays τ_D. One of them is depicted in Fig. 7 with the three measured levels in blue solid line (free-fault case) and red dashed line (with faults). The time occurrence and the duration of the faults are indicated with black arrows. Due to the dynamics of the CFr and the magnitude of the faults, their detection is not obvious.

Table 3. Considered faults

Fault	Magn. [*cm*]	Occurrence (dd:hh:mm)	Duration [*min*]
f_1	-8	01:16:44	200
f_2	1.5	02:14:44	2016
f_3	5	00:01:24	300

The FDI approach is performed by considering the $a_k^{i,i}$ parameters and the predefined thresholds (*see* Table 2). These parameters change during the simulation as depicted for the 25 first simulations and $N_w = 1020$ in Fig. 8. The parameter $a^{1,1}$ crosses the upper threshold after the occurrence of the fault f_1, which allows detecting the occurrence of one fault. The isolation is done by considering which parameter is affected by the fault. Here, the fault f_1 is isolated because the limnimeter L^C is impacted. The detection and isolation of faults f_2 and f_3 is achieved by considering the parameters $a^{2,2}$ and $a^{3,3}$, respectively. The faults are detected when these parameters cross one of the bounds. It can be observed that the generation of the intermittent faults based on random signals has an impact on the estimation of the grey-box parameters. The detection delays τ_D depend clearly on the dynamics of the intermittent faults. However, the faults f_1 and f_3 can be detected after 4 *h* in average, and only the parameter residual fault signals $\phi_k^{a^{j,i}}$ are activated. The detection delay τ_D of f_2 is larger due to its very gradual occurrence.

The average, minimum and maximum detection delays τ_D are computed by considering 500 simulations and the sizes $N_w = 1020$ and $N_w = 1440$. They are presented in Table 4. For a constant fault f_1, a smaller length of the time window leads to smaller detection delays. For intermittent faults, the time window with length $N_w = 1440$ leads to

a better average performance, even if the minimum time delays are perceptibly worse.

Table 4. Detection delay of each fault [*min*]

	$N_w = 1020$			$N_w = 1440$		
Fault	$\lambda\tau_D$	$\min \tau_D$	$\max \tau_D$	$\lambda\tau_D$	$\min \tau_D$	$\max \tau_D$
f_1	217	217	217	247	247	247
f_2	1196	1107	2367	1155	1107	1247
f_3	243	147	387	221	157	447

The knowledge of the navigation schedule is taken into account and leads to $N_w = 1440$ (24 hours). All the dynamics of a navigation day are considered. This value allows meeting the required level of excitation of the inputs and the detection of constant and intermittent faults with very small magnitudes considering real data. The performance of the FDI approach remains good even if a smaller time window ($N_w = 1020$) can improve it in some cases. It is shown that the detection and isolation of constant and intermittent faults can be performed by dealing with the grey-box model parameters.

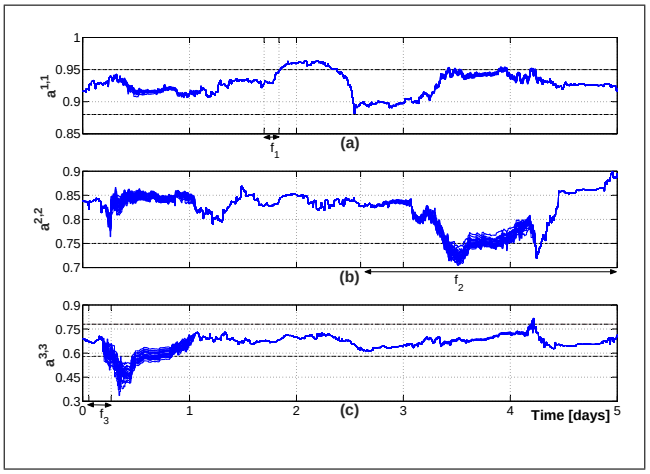

Fig. 8. Value of the $a_k^{i,i}$ parameters (blue) and determined thresholds (black) in the faulty case: (a) $a^{1,1}$, (b) $a^{2,2}$, (c) $a^{3,3}$, for the 25 first simulations.

6. CONCLUSION

A grey-box model-based diagnosis approach for sensor faults on the Cuinchy-Fontinettes reach is proposed in this paper. It allows detecting and isolating constant and intermittent faults by considering the evolution of the grey-box model parameters on sliding windows. Rules for the determination of the sliding window sizes based on the level of excitation of the input signals are proposed. Then, several fault simulations are realized, confirming the good performance of the proposed FDI approach.

REFERENCES

Akhenak, A., Duviella, E., Bako, L., and Lecoeuche, S. (2013). Online fault diagnosis using recursive subspace identification: Application to a dam-gallery open channel system. *Control Engineering Practice*, 21, 797–806.

Bedjaoui, N. and Weyer, E. (2011). Algorithms for leak detection, estimation, isolation and localization in open channels. *Control Engineering Practice*, 19, 564–573.

Blesa, J., Horváth, K., Duviella, E., Puig, V., Bolea, Y., Rajaoarisoa, L., and Chuquet, K. (2014). Model-based sensor supervision in inland navigation networks: Cuinchy-Fontinettes case study. *Journal of Maritime Research*, 11(2), 81–88.

Blesa, J., Puig, V., and Bolea, Y. (2010). Fault detection using interval LPV models in an open-flow canal. *Control Engineering Practice*, 18, 460–470.

Duviella, E., Rajaoarisoa, L., Blesa, J., and Chuquet, K. (2013). Fault detection and isolation of inland navigation channel: application to the Cuinchy-Fontinettes reach. *52nd IEEE Conference on Decision and Control, Florence, Firenze, Italy, 10-13 December*.

Hassanabadi, A.H., Shafiee, M., and Puig, V. (2016). UIO design for singular delayed LPV systems with application to actuator fault detection and isolation. *International Journal of Systems Science*, 47, 107–121.

Horváth, K., Blesa, J., Duviella, E., Rajaoarisoa, L., Puig, V., and Chuquet, K. (2014a). Sensor fault diagnosis of inland navigation system using physical model and pattern recognition approach. *IFAC WC, Cape Town, South Africa, 24-29 August*.

Horváth, K., Duviella, E., Blesa, J., Rajaoarisoa, L., Bolea, Y., Puig, V., and Chuquet, K. (2014b). Gray-box model of inland navigation channel: application to Cuinchy-Fontinettes reach. *Journal of Intelligent Systems*.

Horváth, K., Petreczky, M., Rajaoarisoa, L., Duviella, E., and Chuquet, K. (2014c). MPC of water level in a navigation canal - the Cuinchy-Fontinettes case study. *ECC, Strasbourg, France, 24-27 June*.

Litrico, X. and Fromion, V. (2004). Simplified modeling of irrigation canals for controller design. *Journal of Irrigation and Drainage Engineering*, 130, 373–383.

Ljung, L. (1999). *System identification : theory for the user (2nd Edition)*. Prentice Hall, Upper Saddle River.

Nabais, J.L., Mendonça, L.F., and Botto, M.A. (2012). Sensor fault tolerant architecture for irrigation canals. *10th Portuguese Conference on Automatic Control 16-18 July 2012, CONTROLO2012, Funchal, Portugal*.

Nash, J.E. and Sutcliffe, J.V. (1970). River flow forecasting through conceptual models part I: a discussion of principles. *Journal of Hydrology*, 10(3), 282–290.

Pocher, O.L., Duviella, E., Bako, L., and Chuquet, K. (2012). Sensor fault detection of a real undershot/overshot gate based on physical and nonlinear black-box models. *SAFEPROCESS'12, Mexico, August 29-31*, 8.

Pocher, O.L., Duviella, E., and Chuquet, K. (2011). Sensor fault detection in a real hydraulic system using a classification approach. *ICINCO'11, Noordwijkerhout, Netherlands, 28-31 July*.

Puig, V. and Blesa, J. (2013). Limnimeter and rain gauge FDI in sewer networks using an interval parity equations based detection approach and an enhanced isolation scheme. *Control Engineering Practice*, 21(2), 146–170.

Segovia, P., Blesa, J., Horváth, K., Rajaoarisoa, L., Nejjari, F., Puig, V., and Duviella, E. (2017a). Fault detection and isolation in flat navigation canals. In *4th International Conference on Control, Decision and Information Technologies*, 1–6.

Segovia, P., Rajaoarisoa, L., Nejjari, F., Puig, V., and Duviella, E. (2017b). Decentralized control of inland navigation networks with distributaries: application to navigation canals in the north of France. In *American Control Conference (ACC), 2017*, 3341–3346. IEEE.